Location and dynamics of the Antarctic Polar Front from satellite sea surface temperature data

J. Keith Moore, Mark R. Abbott, and James G. Richman

College of Oceanic and Atmospheric Sciences, Oregon State University, Corvallis

Abstract. The location of the Antarctic Polar Front (PF) was mapped over a 7-year period (1987–1993) within images of satellite-derived sea surface temperature. The mean path of the PF is strongly steered by the topographic features of the Southern Ocean. The topography places vorticity constraints on the dynamics of the PF that strongly affect spatial and temporal variability. Over the deep ocean basins the surface expression of the PF is weakened, and the PF meanders over a wide latitudinal range. Near large topographic features, width and temperature change across the front increase, and large-scale meandering is inhibited. Elevated mesoscale variability is seen within and downstream of these areas and may be the result of baroclinic instabilities initiated where the PF encounters large topographic features. The strong correlations between topography and PF dynamics can be understood in the context of the planetary potential vorticity (PPV or f/H) field. Mean PPV at the PF varies by more than a factor of 2 along its circumpolar path. However, at the mesoscale the PF remains within a relatively narrow range of PPV values around the local mean. Away from large topographic features, the PF returns to a preferred PPV value of $\sim25 \times 10^{-9}$ m^{-1} s^{-1} despite large latitudinal shifts. The mean paths of the surface and subsurface expressions of the PF are closely coupled over much of the Southern Ocean.

1. Introduction

The Antarctic Polar Front (PF), or Antarctic Convergence, marks the location where Antarctic surface waters moving northward sink below subantarctic waters [*Deacon*, 1933]. The PF is a region of elevated current speeds and strong horizontal gradients in density, temperature, salinity, and other oceanographic properties [*Deacon*, 1933, 1937; *Mackintosh*, 1946]. The PF is one of several strong jets within the Antarctic Circumpolar Current (ACC), which flows eastward around Antarctica [*Nowlin and Klinck*, 1986]. North of the PF is the Subantarctic Front (SAF), and to the south is the southern ACC front (SACCF) [*Orsi et al.*, 1995]. The PF marks an important climate boundary in terms of both air-sea fluxes and the heat and salt budgets of the oceans. The path of the PF exhibits considerable variability in the form of mesoscale meandering, eddies, and ring formation [*Mackintosh*, 1946; *Joyce et al.*, 1978]. These mesoscale processes are likely important in meridional fluxes of heat and salt within the Southern Ocean, yet little is known about their regional and temporal variability [*Nowlin and Klinck*, 1986; *Gouretski and Danilov*, 1994].

We have used the strong gradient in sea surface temperature (SST) across the Antarctic PF to map its location within satellite-derived images of SST over a 7-year period (1987–1993). Satellite data have been used previously to map the PF [*Legeckis*, 1977; *Moore et al.*, 1997] and other strong fronts [i.e., *Hansen and Maul*, 1970; *Olson et al.*, 1983; *Cornillon*, 1986].

The PF has both surface and subsurface expressions whose locations do not necessarily coincide [*Botnikov*, 1963; *Lutjeharms and Valentine*, 1984]. Strong gradients in SST mark the surface expression [*Deacon*, 1933, 1937; *Mackintosh*, 1946].

Subsurface definitions for the PF mark the location where Antarctic surface water moving northward descends rapidly, such as the point where the minimum potential temperature layer sinks below 200-m depth [*Deacon*, 1933, 1937] (see also *Belkin and Gordon* [1996] for a review of PF definitions). South of Africa, the subsurface and surface expressions of the PF are typically separated by distances $<\sim50$ km, although separations of up to 300 km have been noted [*Lutjeharms and Valentine*, 1984; *Lutjeharms*, 1985]. *Sparrow et al.* [1996] conclude that there is a wide separation between the surface and subsurface PF expressions in the vicinity of the Kerguelen Plateau. A similar surface/subsurface split may occur at Ewing Bank [*Moore et al.*, 1997].

Several recent studies have examined the historical data set in an attempt to map the large-scale mean location of Southern Ocean fronts, including the Antarctic PF [*Lutjeharms*, 1985; *Belkin*, 1993; *Orsi et al.*, 1995; *Belkin and Gordon*, 1996; *Sparrow et al.*, 1996]. In addition, *Gille* [1994] used Geosat altimeter data and a meandering jet model to map the mean location of the PF and the SAF. The large changes in sea surface height detected by the two-jet model would likely be associated with the subsurface expression of the PF [*Gille*, 1994]. Comparison of our results with those based on altimeter and in situ subsurface data can provide insights into relationships between the surface and subsurface expressions of the PF.

Strong topographic influence on the ACC and the PF has been noted in numerous studies of the Southern Ocean including analysis of data from ships [*Gordon et al.*, 1978; *Lutjeharms and Baker*, 1980], moorings [*Inoue*, 1985], satellite altimeters [*Chelton et al.*, 1990; *Gille*, 1994], drifting buoys [*Hofmann*, 1985; *Patterson*, 1985], and models [*Johnson and Hill*, 1975; *Killworth*, 1992; *Boyer et al.*, 1993; *Hughes and Killworth*, 1995; *Gille*, 1997]. *Deacon* [1937] argues that the location of the PF is determined by the movements of deep and bottom waters, which are expected to be strongly influenced by topography.

Barotropic flow in the oceans over smoothly varying topography tends to conserve angular momentum by following lines of constant potential vorticity $(f + \zeta)/H$, where f is planetary vorticity, ζ is relative vorticity, and H is ocean depth. In open ocean areas the planetary vorticity is much larger than the relative vorticity, and mean potential vorticity can be approximated as f/H. We use the term planetary potential vorticity (PPV) for this f/H approximation. *Moore et al.* [1997] found that the PPV field strongly influenced the dynamics of the Antarctic PF in the Drake Passage/Scotia Sea region. Here we compare the path of the PF with the PPV field throughout the Southern Ocean.

In the Southern Ocean, large changes in ocean depth associated with the mid-ocean ridges and Drake Passage do not permit the ACC to follow circumpolar lines of constant PPV [*Koblinsky*, 1990]. In these regions the ACC is forced across isolines of PPV, causing inputs of relative vorticity to the water column through the shrinking of vortex lines. This relative vorticity is likely dissipated through nonlinear processes such as eddy action or Rossby waves [*Hughes*, 1995, 1996]. Elevated eddy kinetic energy is seen downstream of major bathymetric features (i.e., Drake Passage and Kerguelen Plateau) [*Daniault and Ménard*, 1985; *Patterson*, 1985; *Sandwell and Zhang*, 1989; *Chelton et al.*, 1990; *Morrow et al.*, 1994].

2. Materials and Methods

Our method for mapping the Antarctic PF has been described in detail by *Moore et al.* [1997], so here we present only a brief description. Daily satellite images of SST at 9 km resolution were obtained from the National Oceanic and Atmospheric Administration (NOAA)/NASA Pathfinder Program, which uses the advanced very high resolution radiometer (AVHRR) sensors on NOAA polar orbiters [*Brown et al.*, 1993; *Smith et al.*, 1996]. Daily satellite passes (both ascending and descending) were composite averaged to produce weekly images of SST. Subsets of these weekly images showing only those areas with strong gradients in SST (gradient maps) were constructed, and the location of the poleward edge of the PF was subjectively digitized by examination of the weekly gradient and SST maps. We defined a strong gradient as a change in temperature across a pixel of $\geq 1.35°C$ over a distance of 45–65 km (depending on latitude and PF orientation) [*Moore et al.*, 1997].

On occasion, two strong gradients in the approximate temperature range and location of the PF were observed. This occurred primarily in two regions, west of Drake Passage and in the southwestern Pacific. When two fronts were observed, the path marked was the one with a temperature structure most similar to the PF upstream and/or downstream from the double front area. If no adjacent data were available, the more poleward front was digitized to better delimit the northward extent of Antarctic surface water. This double-front structure has been noted previously [*Sievers and Nowlin*, 1984; *Read et al.*, 1995]. Sea surface temperature is relatively constant south of the PF, and there is typically not a SST gradient associated with the southern ACC front [*Orsi et al.*, 1995].

The mean path of the PF was determined by first constructing a reference path (a subjective estimate of the mean path) and then calculating the mean deviation of all path points at right angles to this reference path. This mean deviation from the reference path defined the mean path. For most areas a line of constant latitude was used as the reference path. The computed mean path was smoothed (in latitude and longitude) with a 5-point moving boxcar filter.

Two methods were used to quantify variability in the location of the PF. In method 1 the spatial displacement of PF path points at right angles from the mean path was calculated. The root-mean-square (rms) of these spatial displacements is a measure of meandering intensity [*Lee and Cornillon*, 1995]. Method 1 describes large-scale variability, such as that due to latitudinal shifts of the PF. In method 2 the average number of points along the PF was calculated within 1° longitudinal bins and then normalized by the number of path points along the mean path for each bin. This method is a measure of mesoscale variability, or path curvature, relative to the mean path where such mesoscale variability has been smoothed out. When calculating the average number of path points per bin, paths with fewer points than the mean path minus 3 were excluded as incomplete.

To quantify the temperature gradient across the front, we began at the poleward edge of the PF and moved up the temperature gradient until SST did not increase over a 3-pixel (∼20–30 km) distance or until a missing pixel was reached. The same method was used to measure the width of the front. Only complete transects were used to calculate the mean temperature change and distance across the PF. We defined the seasons as spring (weeks 38–50), summer (weeks 51, 52, and 1–10), fall (weeks 12–24), and winter (weeks 25–37).

A high-resolution predicted seafloor topography, derived from ship and Geosat altimeter data [*Smith and Sandwell*, 1994], was used to create maps of bathymetry and planetary potential vorticity for comparison with PF paths. The topography had a grid spacing of 3 min of longitude by 1.5 min of latitude, which was remapped to the same resolution as the SST data. These bathymetry data were also used to calculate the slope of the ocean floor across the PF and depth at the PF over a 90-km wide swath.

We have included some discussion of interactions between the PF and the SAF. The SAF is defined as the maximum SST gradient in the temperature range of 5°–9°C [*Burling*, 1961]. *Lutjeharms and Valentine* [1984] found the mean SST range for the SAF between 20°W and 40°E to be 5.1°–9.0°C (see also *Belkin and Gordon* [1996] for a review of SAF definitions).

3. Results

The position of the Antarctic PF was mapped from weekly SST images over a 7-year period 1987–1993 (Figure 1). It is apparent that there are large regional variations in both the latitudinal range of the PF and in the number of paths digitized. We will demonstrate that these regional variations are primarily a function of the underlying topography and the corresponding PPV field. Relatively few paths were digitized in areas above the deep ocean basins (i.e., 120°–90°W, 50°–70°E, and 110°–140°E; see Figure 1).

3.1. Topography and the Mean Path of the PF

Our mean path for the Antarctic PF is shown in Plate 1 over the topography of the Southern Ocean. The strong influence of topography on the mean path of the PF is readily apparent. The PF follows closely the Pacific-Antarctic Ridge, the Falkland Plateau, parts of the Mid-Atlantic and Southeast Indian Ridges, and the steeply sloped topography associated with the Ob'-Lena Rise (40°–45°E) and Kerguelen Plateau (75°–80°E) (Plate 1).
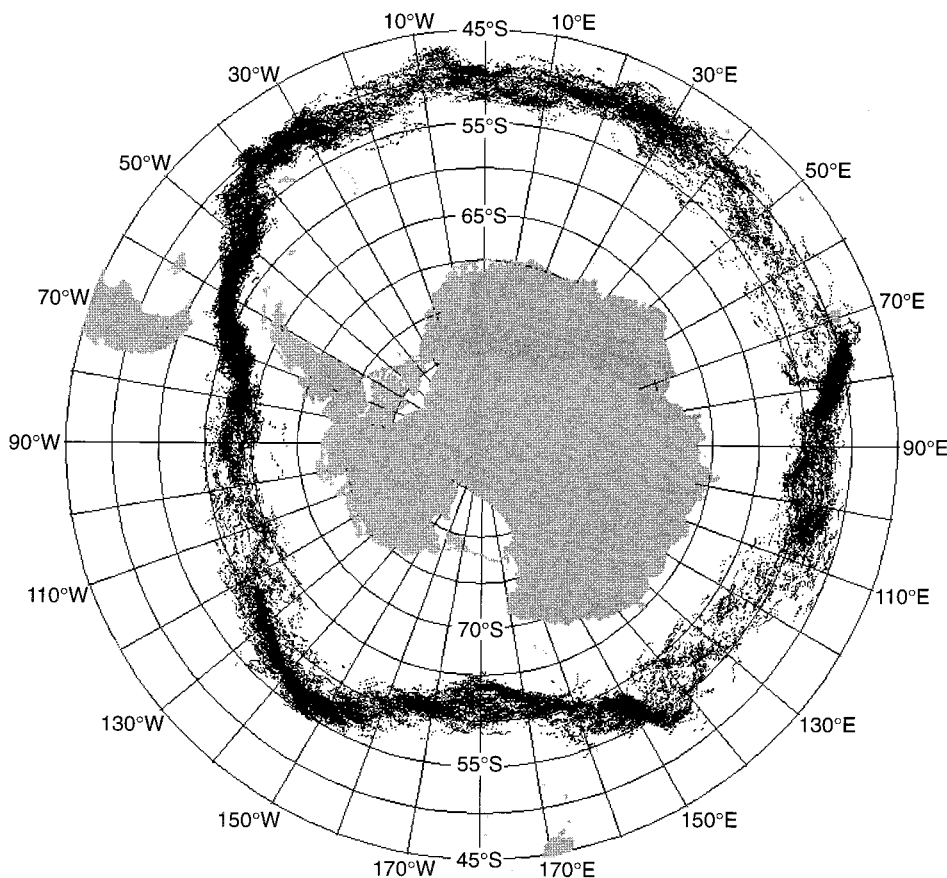
Figure 1. Displayed are all paths for the Antarctic Polar Front digitized for the years 1987–1993.

Our mean path follows the Pacific-Antarctic Ridge in the SW Pacific, crossing just south of the Udintsev Fracture Zone (UDF) at ~145°W. The SAF was observed frequently to merge with the PF and also pass through the UDF. At other times the SAF remained farther north, crossing the ridge at the Eltanin Fracture Zone. These observations are consistent with previous studies [*Belkin*, 1988; *Patterson and Whitworth*, 1990; *Orsi et al.*, 1995]. After crossing the ridge the PF flows to the southeast until it encounters the Antarctic Peninsula at ~78°W.

We have previously described the mean path of the PF through the Drake Passage/Scotia Sea region [*Moore et al.*, 1997]. The mean path is largely constrained by topography through the Drake Passage (especially at ~62°–57°W [see *Moore et al.*, 1997] and along the Falkland Plateau. There is an area of high variability and intense meandering in the northern Scotia Sea [*Gordon et al.*, 1977; *Chelton et al.*, 1990; *Moore et al.*, 1997].

After crossing the Mid-Atlantic Ridge at ~10°–9°W the PF flows eastward near 50°S dipping southward at ~30°E, in general agreement with previous studies [*Lutjeharms and Valentine*, 1984; *Lutjeharms*, 1985; *Belkin*, 1993; *Gille*, 1994; *Orsi et al.*, 1995; *Belkin and Gordon*, 1996]. Our mean path dips southward from ~5° to 11°E. In this region the PF was often located near the Mid-Atlantic Ridge along ~53°S (Figure 1 and Plate 1). *Lutjeharms and Valentine* [1984] show a number of PF crossings at this steeply sloped topography (see also *Belkin*, [1993, Table 4]).

In the area around ~30°E the PF often displayed intense meandering such that a clear path could not be determined,

similar to the high variability area in the northern Scotia Sea [see *Moore et al.*, 1997]. *Gouretski and Danilov* [1993, 1994] have shown that the PF regularly spawns warm core rings in this region. Other studies have found elevated eddy variability near 30°E [*Daniault and Ménard*, 1985; *Sandwell and Zhang*, 1989; *Chelton et al.*, 1990; *Morrow et al.*, 1994; *Gille*, 1994]. Dynamic height contours also pinch closer together here [*Gordon et al.*, 1978; *Gamberoni et al.*, 1982]. *Deacon* [1937] suggests the PF is deflected southward by the ridge system at ~30°–31°E (see Plate 1). We also observed interaction with the SAF in this area, as has been reported previously [*Orsi et al.*, 1993; *Read and Pollard*, 1993; *Belkin and Gordon*, 1996].

The SAF appears to have a bimodal path distribution beginning at ~30°E. The SAF often turns northward upon encountering the steep ridge extending southward from the Crozet Plateau (along ~30°–31°E; see Plate 1), turning eastward and converging with the South Subtropical Front (SSTF) and, farther east, the Agulhas Front to form the "Crozet Front" north of Crozet Plateau [*Park et al.*, 1993; *Belkin and Gordon*, 1996; *Sparrow et al.*, 1996]. Alternatively, the SAF is forced south of the steep ridge near 30°E, forcing it into close proximity with the PF. On this southern route the SAF flows along the southern side of the Crozet Plateau before turning northward just east of Crozet Island, joining the Crozet Front north of Crozet Plateau [*Orsi et al.*, 1993, 1995; *Gille*, 1994]. We observed the SAF following both routes through this area.

Our mean path turns southward at the Ob'-Lena Rise (~46°E). A phenomenon described by *Sparrow et al.* [1996], who conclude that there is a persistent split here between the
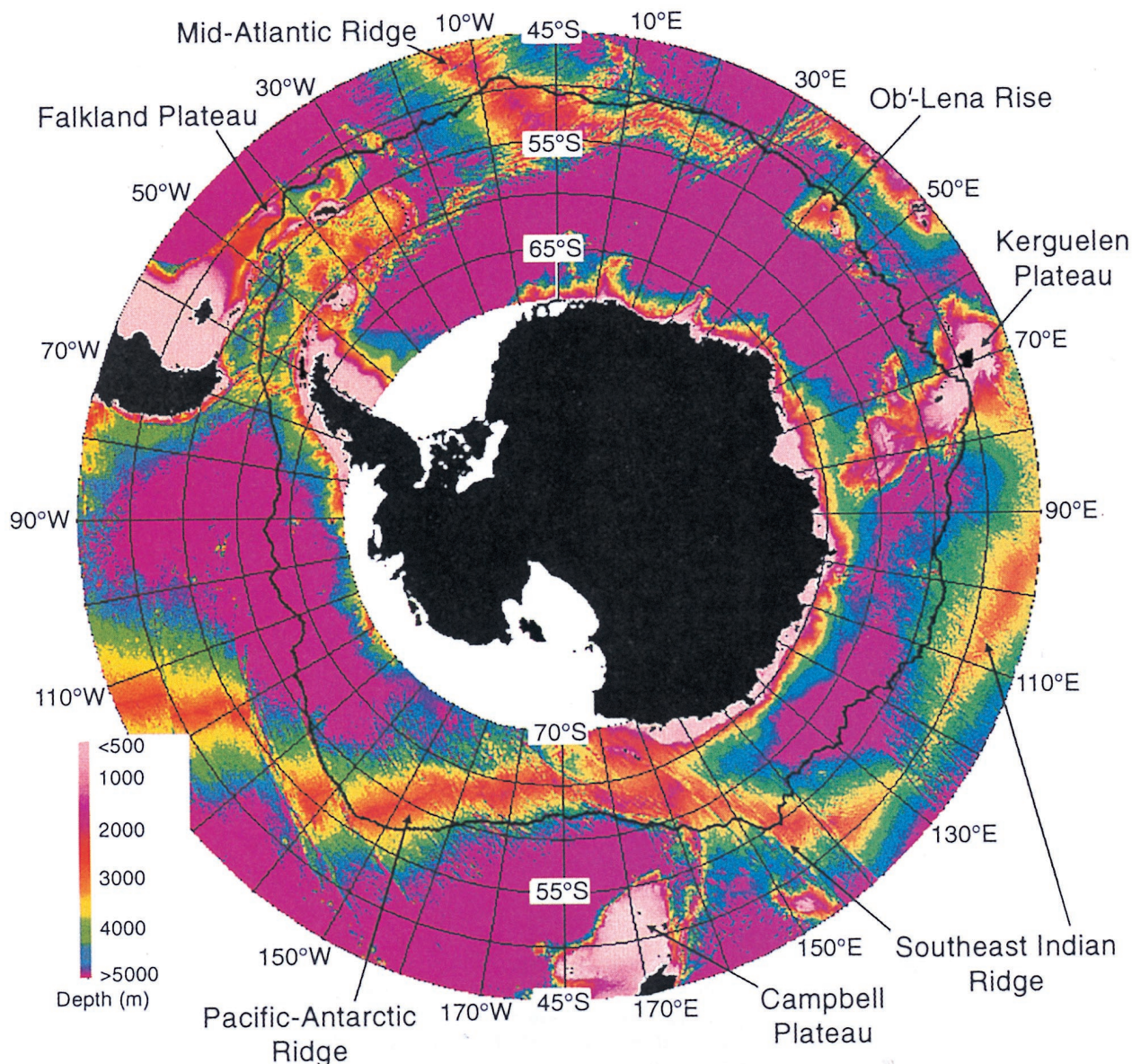
Plate 1. The calculated mean path for the Antarctic Polar Front is shown over the topography of the Southern Ocean [*Smith and Sandwell*, 1994].

surface and subsurface expressions of the PF, with the subsurface expression passing north of Kerguelen Island and the surface expression moving southward to cross the Kerguelen Plateau through an area of deeper bathymetry at ~56°–57°S. We mapped the PF passing through this gap at ~56°–57°S, which is called the 77°E Graben [*Schlich et al.*, 1987], on a number of occasions (compare Figure 1 and Plate 1). However, we also mapped the PF over a wide range in this region (spanning nearly 10° of latitude), including, at times, north of Kerguelen Island (Figure 1 and Plate 1).

Previous studies have placed the surface expression of the PF over a wide latitudinal range in the Kerguelen region [*Gamberoni et al.*, 1982; *Deacon*, 1983; *Klyausov*, 1990; *Park et al.*, 1993; *Belkin and Gordon*, 1996; *Sparrow et al.*, 1996]. The path of *Sparrow et al.* [1996] likely marks the southern limit of the PF surface expression. In addition, few PF paths were marked in the region between the Ob'-Lena Rise and the Kerguelen Plateau, even under cloud-free conditions (Figure

1). Thus, in our analysis, there frequently was no detectable surface expression of the PF between the Ob'-Lena Rise and Kerguelen Plateau.

East of Kerguelen Plateau, the envelope of PF paths narrows sharply by 80°E (Figure 1), and the mean path moves to the south following closely the eastern flank of Kerguelen Plateau (Figure 1 and Plate 1). The PF turns to the northeast at ~95°E and follows the southern flank of the Southeast Indian Ridge (~100°–110°E) before moving southeastward again at ~110°E (Plate 1). The PF moves northward again while crossing the Southeast Indian Ridge at ~145°E and then closely follows the topography into the Pacific (Plate 1).

3.2. Comparisons With Previous Results

In general, our mean path for the PF is in good agreement with the mean paths of *Gille* [1994], *Orsi et al.* [1995], and *Belkin and Gordon* [1996], all based on subsurface markers of the PF (Plate 2). This indicates that while the location of
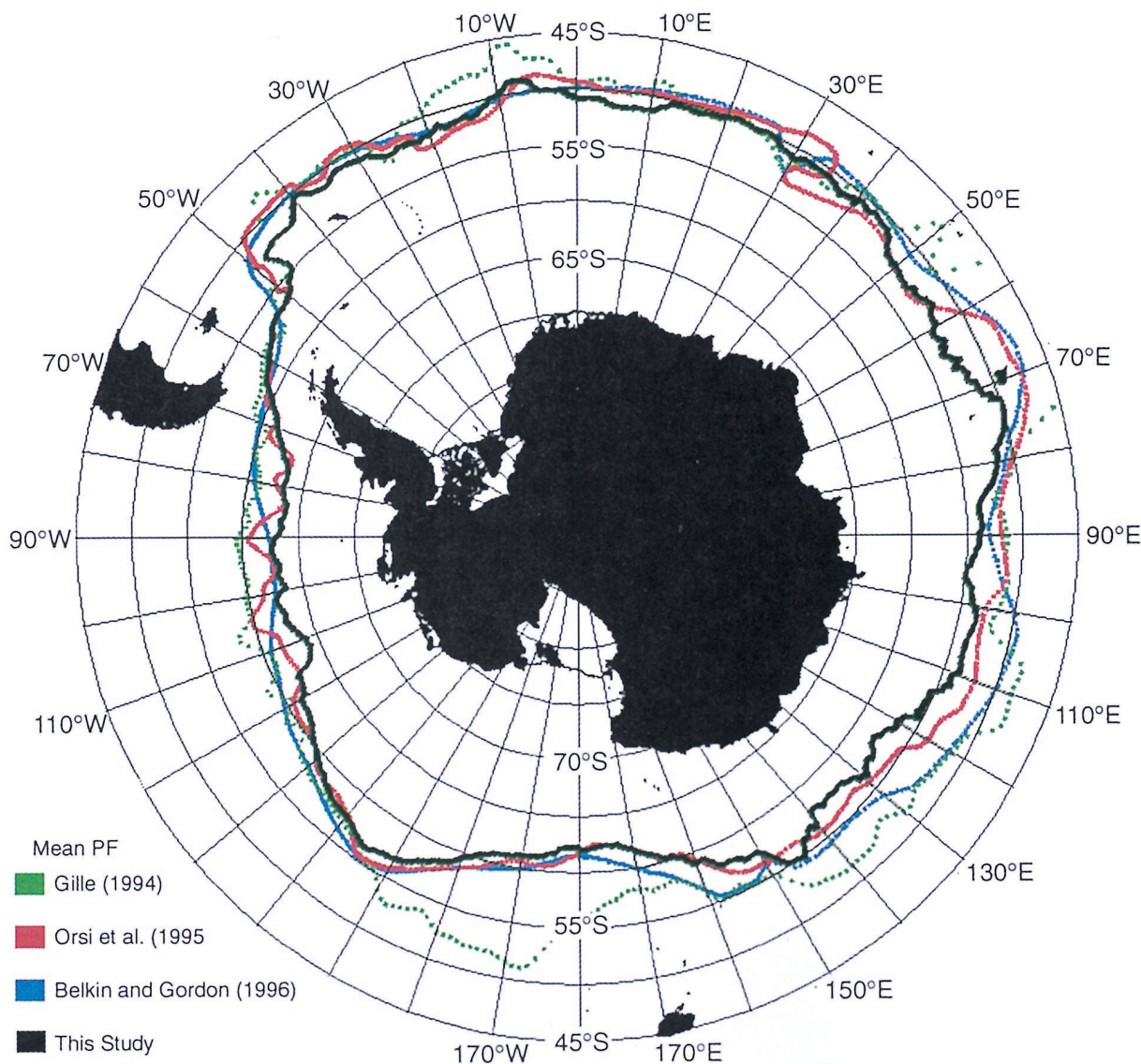
Plate 2. Our mean path for the Antarctic Polar Front (black line) compared with the mean paths of *Gille* [1994] (dotted green line), *Orsi et al.* [1995] (red line), and *Belkin and Gordon* [1996] (blue line).

subsurface and surface expressions of the PF may differ over short timescales, their mean location is closely coupled over much of the Southern Ocean.

Our PF path agrees very well with the paths of *Orsi et al.* [1995] and *Belkin and Gordon* [1996] in the vicinity of large bathymetric features, such as along the Pacific-Antarctic Ridge (typically separated by <1° of latitude; Plate 2). The four PF mean paths in Plate 2 are in closest agreement in several areas where topographic steering of the front is particularly strong (~140°–148°W, ~65°–50°W, 40°–45°E, and from ~76° to 81°E; compare Plates 1 and 2). The distances separating the paths increase over deep basin areas (115°–85°W, 25°–40°E, 55°–65°E, and 90°–140°E) and in the vicinity of Kerguelen Plateau and Ewing Bank on the Falkland Plateau, where there may be frequent surface/subsurface separations [*Sparrow et al.*, 1996; *Moore et al.*, 1997].

A survey of the literature revealed a number of instances where a ship crossed the Antarctic PF at approximately the same time (within 2 weeks) as our satellite mapping of the PF

(see Table 1). Our location for the PF is typically south of the ship-determined locations, on average 0.7° of latitude. Our PF location marks the poleward edge of the front, which is ~35–55 km wide. This indicates a small mean southward displacement, albeit with considerable variability (Table 1). *Lutjeharms and Valentine* [1984] report the surface expression as south of the subsurface expression 75% of the time in the region south of Africa.

Peterson and Whitworth [1989] present data from several crossings of the subsurface expression of the PF in the SW Atlantic for two periods (see Table 1). The surface expression of the PF is typically not present in their transects, generally being located farther south. During both time periods the distance separating the surface and subsurface expressions of the PF is small near 41°W and increases in areas farther east (Table 1). This is consistent with previous results [*Deacon*, 1933; *Guretskii*, 1987].

The mean temperature change across the front over the 7-year period was 1.44°C across an average width of 43 km.
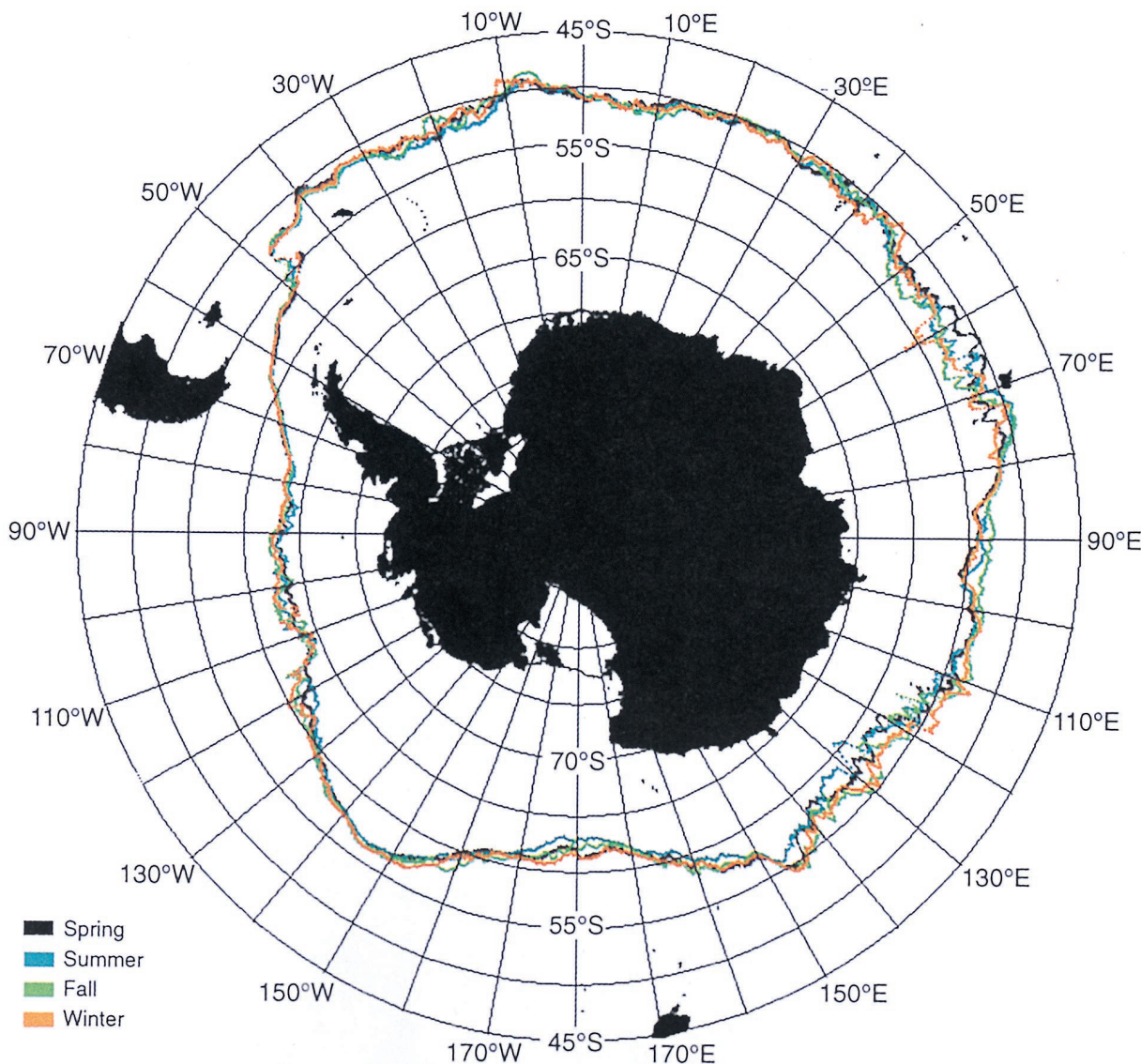
Plate 3. The seasonal mean paths of the Antarctic Polar Front are displayed.

This cross-frontal temperature change is somewhat less than previous estimates (1.7°C [*Mackintosh*, 1946], 1.8°C south of Africa [*Lutjeharms*, 1985], 1.9°–2.0°C in the southwest Atlantic, [*Guretskii*, 1987], 1.6°C (35°–49°E), 1.9°C (97°–112°E) [*Belkin*, 1989], and 1.7°C for the region 90°–20°W [*Moore et al.*, 1997]). Our lower estimate is likely due to better spatial resolution (~9 km) than most ship transects and increased sampling over ocean basin areas where the SST gradient is typically weaker. Our mean PF width of 43 km agrees well with the 44 km estimate of *Gille* [1994] and the 40 km estimate of *Sciremammano et al.* [1980]. The mean spatial rms displacement was 136 km. This is higher than the value of 100 km reported previously for the Drake Passage/Scotia Sea region [*Moore et al.*, 1997]. Mean PPV along the mean path of the PF was 32.08×10^{-9} m^{-1} s^{-1}. There were large regional variations in all of these parameters of the PF.

3.3. Spatial Variability

The spatial rms displacement of Antarctic Polar Front (PF) path points at right angles from the mean path was calculated (Figure 2). Comparing Plate 1 and Figure 2, it can be seen that variability in the location of the PF is highest over deep basin areas (120°–90°W, 30°–10°W, 30°–70°E, and 90°–140°E). Variability is lower near large bathymetric features, where the ocean floor is steeply sloped (at the mid-ocean ridges, near 78°W at the Antarctic Peninsula, within Drake Passage, along the Falkland Plateau, and east of Kerguelen Island along the Kerguelen Plateau; Plate 1 and Figure 2).

The regional variability apparent in Figures 1 and 2 can be quantified if we examine the behavior of the PF averaged over 5° longitudinal bins (Figure 3). For this statistical analysis the region 50°–45°W has been divided into two bins north and south of the North Scotia Ridge (this ridge separates two different domains; see Figure 1 and Plates 1 and 2; see also *Moore et al.* [1997]). All cross-correlation coefficients given for Figure 3 are significant at the 95% confidence level by Student's *t* test, (except where noted otherwise).

There is a strong positive correlation between the temperature change across the front and the width of the PF (Figures 3a and 3b, cross-correlation coefficient of 0.73). *Gille* [1994] reported that the width of the PF varied by ~20% over large spatial scales. We observed a similar variability in frontal width
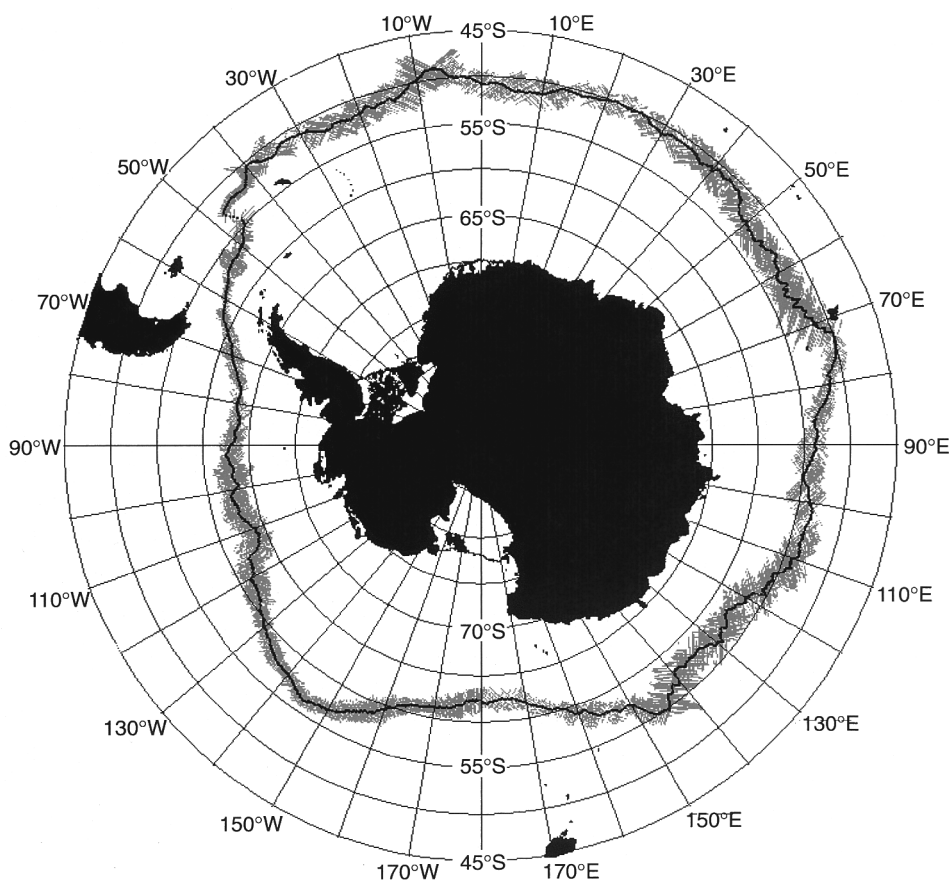
Table 1. A Comparison of the Position of the Antarctic Polar Front (PF) from ship Transects (Subsurface and Surface Location) and With Our Satellite-Derived Surface Position at Approximately the Same Time (Within 2 Weeks)

Reference (PF Crossing)	Longitude	Subsurface	Surface	Satellite (week)
Read et al. [1995, Figures 4–7]				
(Nov. 14, 1992)	~56°W	57.8°S	58.2°S	58.7°S (Nov. 5–11 and Nov. 12–18)
(Dec. 11, 1992)	~88°W	61.5°S	61.5°S	63.9°S (Dec. 17–23)
Peterson and Whitworth [1989, Figure 11]				
(March 22 to April 5, 1997)	~41.2°W	49.3°S	···	49.6°S (March 26 to April 1)
	~39°W	49.3°S	···	49.8°S, 50.8°S (March 19–25 and March 26 to April 1)
(April 5–16, 1987)	~41°W	49.3°S	···	49.7°S (April 2–8)
	~39°W	49.3°S	···	50.3°S (April 2–8)
	~38°W	49.0°S	···	50.7°S (April 2–8)
Ikeda et al. [1989, Figure 4]				
(March 12–20, 1987)	~54°W	56.4°S	···	56.5°S, 56.4°S (March 5–11 and 11–17)
Tsuchiya et al. [1994, Figure 2]				
(Feb. 13, 1989)	~33°W	49.5°S	~49.0°–50.0°S	50.6°S (Feb. 12–18)
Laubscher et al. [1993, Figure 5]				
(first half Dec. 1990)	~4°W	···	~48.8°–49.5°S	50.9°S, 52.3°S (Dec. 10–16 and 17–23)
(mid-Feb. 1991)	~27°W	···	~49.3°–50.3°S	53.4°S, 52.7°S (Jan. 29 to Feb. 4 and Feb. 12–18)
Robertson and Watson [1995, Figure 5]				
(Feb. 11–12, 1993)	~20°E	···	51.0°–51.6°S	51.0°S (Feb. 12–18)

Week of satellite observation given as year (first two digits) and week (second two digits). Where possible, the date of the in situ PF crossing was obtained from the authors of the listed references.

(Figure 3b). Both temperature change and width of the PF were inversely correlated with meandering intensity as measured by the spatial rms displacement (Figures 3a, 3b, and 3c; cross-correlation coefficients of −0.65 and −0.54, respectively). Both temperature change and width of the front were also inversely correlated with ocean depth (Figures 3a, 3b, and 3e; cross-correlation coefficients of −0.19 (not significant at the 95% confidence level) and −0.46, respectively).

Figure 2. The mean path of the Antarctic Polar Front plus or minus the root mean square of the spatial displacements of Antarctic Polar Front path points at right angles to the mean path is shown.
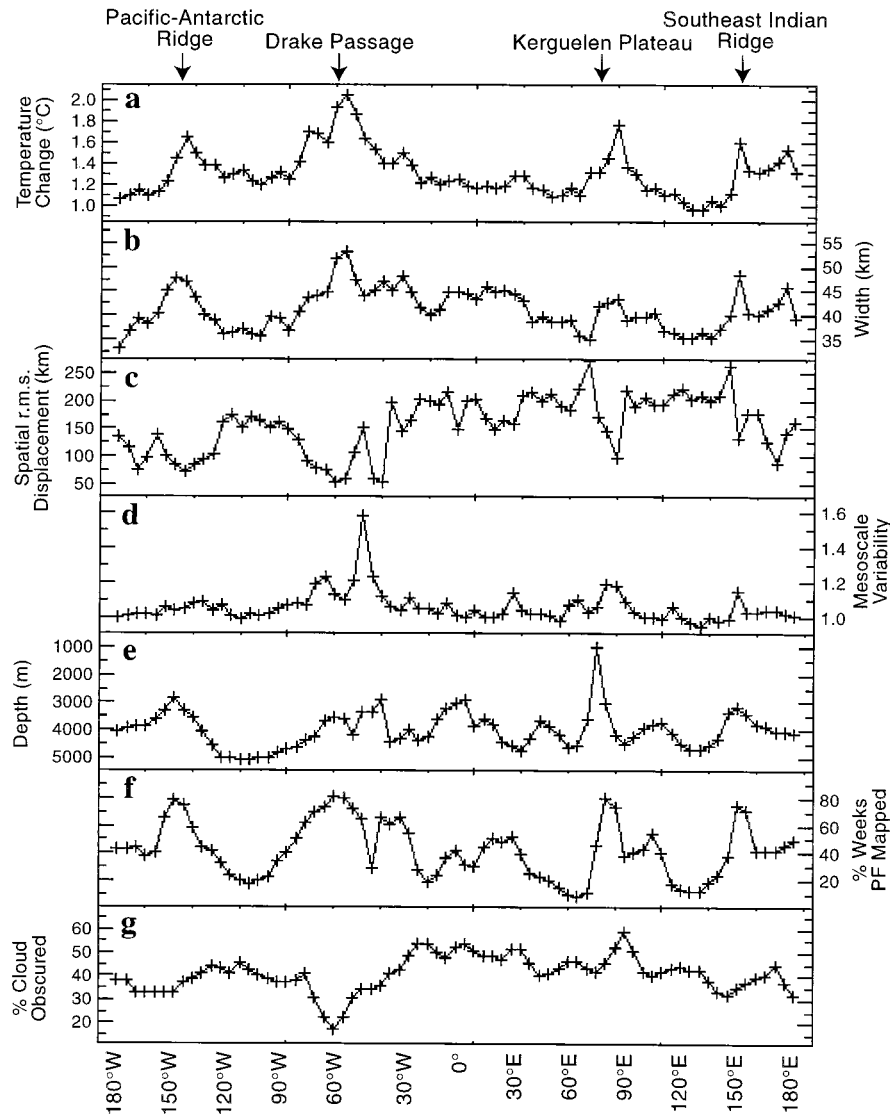
Figure 3. Displays are some statistical properties of the Antarctic Polar Front averaged over 5° longitudinal bins. Temperature change across the (a) front, (b) frontal width, (c) spatial rms displacement, (d) mesoscale variability (relative units, see text for details), (e) ocean depth, (f) percentage of weeks some portion of the PF was mapped, and (g) percentage of pixels between 45° and 65°S with no data in our weekly images because of persistent cloud cover are shown.

The PF is intensified (increased width and temperature change across the front) at major bathymetric features, including the Pacific-Antarctic Ridge, Drake Passage, the Kerguelen Plateau, and crossing the Southeast Indian Ridge (Plate 1, Figures 3a, 3b, and 3e). An exception was the Mid-Atlantic Ridge, where there was no intensification (Figures 3a, 3b, and 3e). Dynamic height contours typically pinch together in these regions [*Gordon et al.*, 1978]. *Gille* [1994] found that the total height difference across the PF and SAF increased where the ACC crossed topographic features. This relationship between topography and temperature change across the front is apparent in the data of *Mackintosh* [1946], with weaker gradients overlying the ocean basin areas. *Emery* [1977] noted that ACC fronts were broad and diffuse in the southeast Pacific, where no large topography acts to concentrate the ACC flow. The strength of the SST gradient (temperature change divided by frontal width) also increased in these areas associated with

large topographic features. Gradient strength averaged over 5° longitudinal bins ranged from 2.6° to 4.1°C/100 km and was strongest just downstream of Kerguelen Plateau.

The intensification of the PF associated with major bathymetric features persists for some distance downstream. In fact, three parameters (width, temperature change across the front, and the percentage of weeks the front was mapped; Figures 3a, 3b, and 3f) had higher cross-correlation coefficients with ocean depth (Figure 3e) when they lagged depth by one longitudinal bin. The cross correlations for Figures 3a, 3b, and 3f lagging Figure 3e by 1 were −0.27, −0.50, and −0.54 (all significant and all higher than with no lag). Thus increased cross-frontal widths and temperature gradients are seen downstream of the Pacific-Antarctic Ridge (~135°–128°W), Drake Passage (~55°–45°W), Kerguelen Plateau (~79°–86°E), and the Southeast Indian Ridge (~150°–155°E; see Plate 1 and Figure 3).

It is in these areas of intensification associated with major

bathymetric features that we see elevated mesoscale variability at the PF (Figure 3d). Mesoscale variability was strongly correlated with cross-frontal temperature change and width (cross correlations for Figure 3d with Figure 3a and 3b were 0.61 and 0.40, respectively). Mesoscale variability was also significantly correlated with depth when it lagged depth by one bin (cross correlation for Figure 3d lagging Figure 3e by one bin of −0.20). We also observed the formation of warm and cold core rings at the PF most frequently in these areas just downstream of large topographic features (ring formation at the PF will be discussed in detail elsewhere). Altimeter, hydrographic, and drifter studies of the Southern Ocean have also found high eddy variability in these areas [*Lutjeharms and Baker*, 1980; *Daniault and Ménard*, 1985; *Chelton et al.*, 1990; *Morrow et al.*, 1990; *Gouretski and Danilov*, 1994; *Gille*, 1994].

The intensification of the PF may lead to baroclinic instabilities and eddy/ring formation in these regions. Mesoscale variability was also highly correlated with the strength of the SST gradient across the PF when it lagged gradient strength by one longitudinal bin (cross correlation of 0.52). Gradient strength is a measure of vertical shear within the PF. Baroclinic instabilities are more likely in areas of increased shear. Mesoscale variability was also significantly correlated with PPV when lagging PPV by one longitudinal bin (cross correlation of 0.22). This suggests that the relative vorticity put into the water column where the topography forces changes in PPV is dissipated downstream by eddy and ring formation. *Witter and Chelton* [1998] studied the effects of zonal-varying topography on a meandering jet with a quasi-geostrophic channel model. Eddy kinetic energy and the growth rate of instabilities reached their maximum downstream of zonal variations in topography in regions of reduced ambient vorticity gradients [*Witter and Chelton*, 1998]. The increase in frontal width associated with crossing major bathymetric features resembles the "supercritical to subcritical" transition described by *Pratt* [1989].

Note the strong correlations between the percentage of weeks that some portion of the PF was mapped and the change in temperature across the PF, the width of the PF, and ocean depth (Figures 3f, 3a, 3b, and 3e; cross-correlation coefficients of 0.74, 0.76, −0.42, respectively). The PF was mapped most frequently in areas where the PF was intensified. The SST gradient was easier to detect in these areas. Fewer paths were mapped over the deep ocean basins (Figures 3e and 3f). In these areas the PF SST gradient is weakened (Figures 3a and 3b), often making it difficult to distinguish from the background meridional temperature gradient. Figure 3g shows the mean percentage of pixels (45°–65°S) with no data in our weekly images because of persistent cloud cover. Drake Passage consistently had the least cloud-masked areas (17.5%), while a maximum in cloud cover of 59.2% was seen 85°–90°E. Our PF coverage was correlated with this measure of cloudiness (Figures 3f and 3g; cross correlation of −0.43). This correlation is significant at the 95% confidence level, but it is weaker than the correlations with frontal intensity. Thus, despite persistently cloudy conditions over the Southern Ocean our temporal coverage in most areas was limited by the strength of the SST gradient.

3.4. Temporal Variability

Mean temperature at the poleward edge of the PF for several regions is displayed in Figure 4. In general, springtime warming is relatively rapid, with a more gradual cooling during the fall, a pattern observed by *Mackintosh* [1946]. The mean seasonal cycle at the poleward edge of the PF varies from ~2.8°C during the summer to ~0.4°C in the winter (Figure 4a). *Houtman* [1964] calculated a mean summer/winter temperature difference of 2.1°C for a constant latitude. *Lutjeharms and Valentine* [1984] gave a mean poleward edge temperature of 2.5°C from mainly summertime crossings of the PF south of Africa.

Weakest seasonality was seen where the PF was at lower latitudes (Figure 4b). Seasonality was greater at high latitudes (Figure 4c). Lowest winter temperatures were seen just west of Drake Passage (80°–65°W), where SST at the PF at times approached the freezing point of seawater (Figure 4d). The cold temperatures observed in this area likely reflect substantial amounts of sea ice entering the PF. The maximum extent of the seasonal ice sheet can reach the PF during austral winter in this region [*Gloersen et al.*, 1992]. SST was consistently higher (~1°C) in the region just to the east (65°–45°W, Figure 4e).

Seasonal variations in the properties of the PF were relatively small compared with the spatial variability (Figure 5). The PF mean width and temperature gradient were highest during the spring (44.4 km and 1.53°C; Figures 5a and 5b). Weakest seasonal gradients and narrowest frontal widths were observed during the fall (1.37°C and 42.6 km). Mean latitude was farthest south during the winter at 57.0°S and at lowest latitudes during the fall at 55.9°S (Figure 5d). Spatial rms displacements were higher during the summer and fall (140 and 142 km, respectively). Meandering intensity was lower during winter and spring (spatial rms displacement of 130 km for both seasons). There is an inverse relationship between spatial rms displacements and both width and temperature change across the front. Fewer PF paths were mapped during fall and winter compared with the spring-summer period (Figure 5f).

In areas where the Antarctic PF was mapped along the same longitudinal line in successive weeks an average weekly latitudinal shift of 22 km was calculated (*n* = 174). A maximum shift of 177 km was observed in the northern Scotia Sea [*Moore et al.*, 1997]. Note that temporal coverage of the PF was better in low-variability areas (Figure 3c and 3f); thus our value of 22 km may be an underestimate.

Seasonal variability in the location of the PF was qualitatively similar to the spatial variability described above (Plate 3). Seasonal variability was low where topographic steering of the PF is strong, and it was higher over the deep ocean basins (Plates 1 and 3). Some seasonality was observed in the area from ~175°E to 170°W; the PF moved southward during the summer and farthest north during winter. These seasonal shifts may be due to the influence of the seasonal ice sheet extending from the Ross Sea. A southward shift of the surface PF relative to the subsurface expression has been documented south of Africa (0°–30°E) during austral summer [*Lutjeharms and Mc-Quaid*, 1986; *Lutjeharms and Foldvik*, 1986]. This may not always be the case, however, as our seasonal mean paths do not show a mean southward shift during summer in this region (Plate 3). Our mean path is south of those *Orsi et al.* [1995] and *Belkin and Gordon* [1996] in this region, perhaps indicating that the surface expression is frequently south of the subsurface position (Plate 2).

Variability at interannual timescales was also strongly influenced by the underlying topography (Plate 4). The annual mean paths are in close agreement where topographic effects
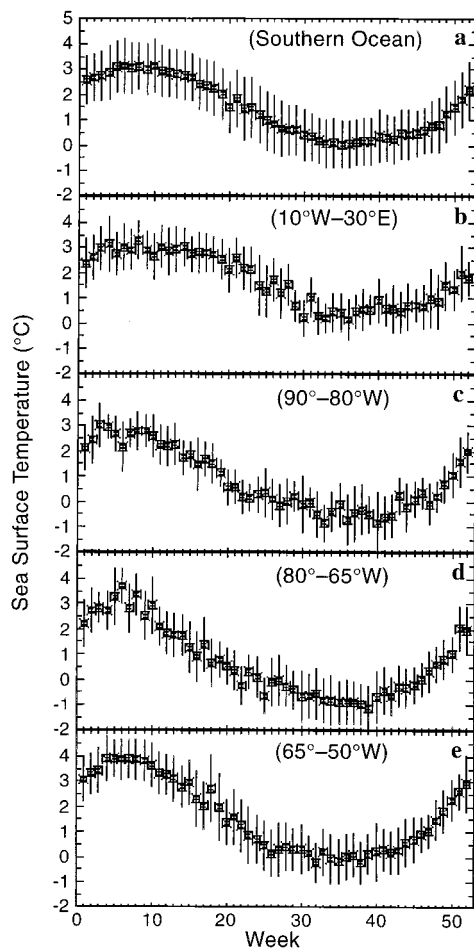
Figure 4. The seasonal cycle of sea surface temperature (SST) at the poleward edge of the Antarctic Polar Front is shown for selected regions: (a) the circumpolar mean, (b) 10°W–30°E, (c) 90°–80°W, (d) 80°–65°W, and (e) from 65°–50°W. Error bars show ±1 standard deviation.

on the PF are strongest (~148°–150°E, ~145°–140°W, through much of the Drake Passage/Scotia Sea region, ~15°–20°E, and ~75°–85°E; Plates 1 and 4). Interannual variability was also elevated above the deep ocean basins (Plate 4). *Chelton et al.* [1990] found that mesoscale variability in the ACC was strongly influenced by topography and showed little temporal variability over seasonal or interannual timescales.

3.5. Planetary Potential Vorticity at the PF

PPV does not remain constant along the mean path of the PF (Figure 6a). It can be seen in Figure 6 that despite large latitudinal shifts along the mean path of the PF, PPV is largely a function of the underlying topography (Figures 6a and 6c; cross-correlation coefficient of −0.75). PPV increases and the PF moves equatorward each time it is forced into areas of decreasing ocean depth (Figures 6a, 6b, and 6c). After crossing each topographic feature the front turns poleward, and PPV returns to a relatively constant value of ~25 × 10⁻⁹ m⁻¹ s⁻¹ despite large latitudinal shifts (Figure 6). The bottom slope across the PF was significantly correlated with the temperature change across the front, frontal width, and mesoscale variability (cross correlations between Figure 6d and Figures 3a, 3b, and 3d of 0.31, 0.45, and 0.35, respectively).

The dynamics driving much of the observed spatial and temporal variability in the location of the PF can be understood if we examine the mean path of the PF in the context of the PPV field. In Plate 5 the mean path of the PF is shown overlain on a map of PPV. The mean PPV along the PF has been calculated within a moving 2° of longitude window. Along each line of longitude a relatively narrow range of PPV values
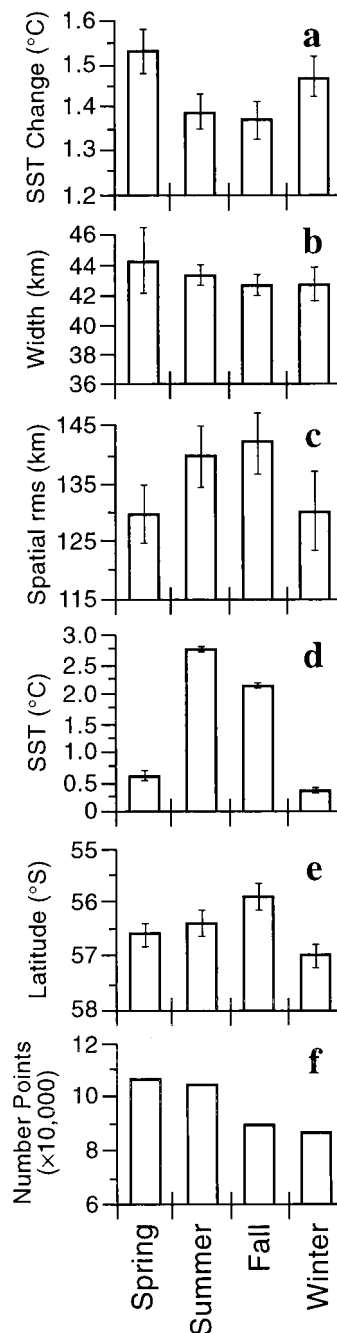

Figure 5. Seasonal mean values for several properties of the Antarctic Polar Front are shown. Displayed values include the temperature change across (a) the front, (b) the width of the front, (c) the mean spatial rms displacement at right angles to the mean path, (d) the mean sea surface temperature, (e) the mean latitude, and (f) the number of path points digitized. Error bars indicate ±1 standard error assuming each weekly image is an independent sample (*n* = 364).
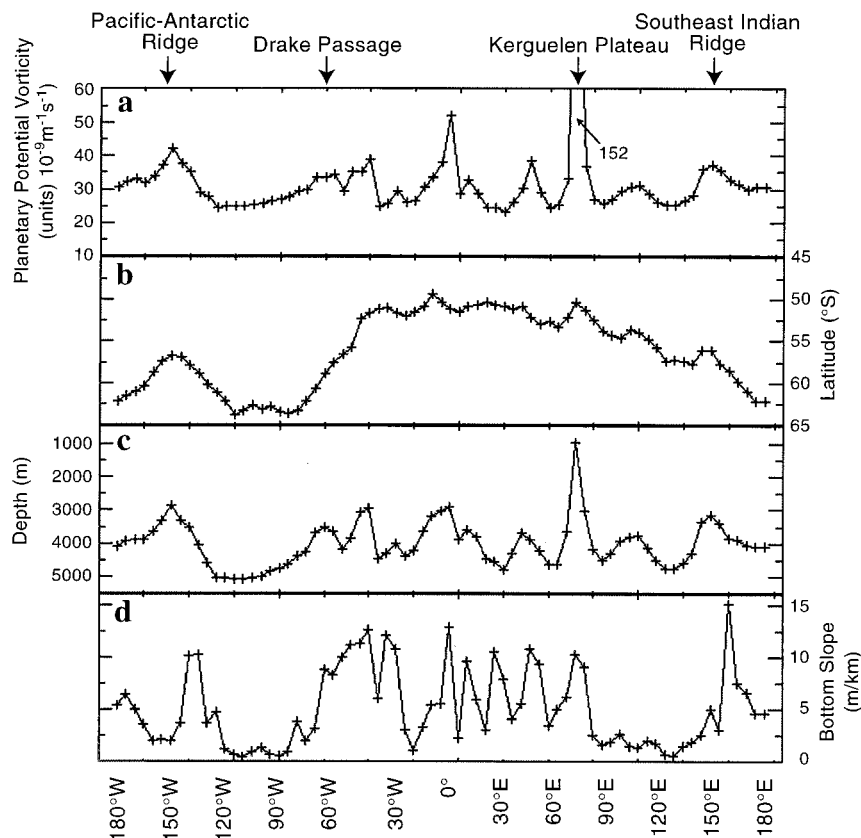
Figure 6. Displayed are some statistical properties of the Antarctic Polar Front averaged over 5° longitudinal bins. The average planetary potential vorticity along the mean path of (a) the PF, (b) the latitude, (c) the ocean depth, and (d) the slope of the ocean floor across the PF at right angles to the flow direction are shown.

around this running mean value is shown in white. This range consists of the mean value plus or minus two units of 10^{-9} m^{-1} s^{-1}. This corresponds to the mean value ±~7%. This range of values shown in white can be considered a local plain of quasi-constant PPV [see *Moore et al.*, 1997].

Comparing Figure 1 and Plate 5, it can be seen that the envelope of PF paths corresponds with the size and shape of this plain of quasi-constant PPV. The broad plains in PPV associated with the ocean basin areas (~130°–80°W, 25°–10°W, 52°–65°E, and 85°–140°E) are precisely the areas where the envelope of PF paths widens (Figure 1 and Plate 5). Variability in the location of the PF was highest at all temporal scales over these broad PPV plains (Figures 2 and 3, Plates 3 and 4). In these areas the PF can meander substantially while maintaining a relatively constant PPV. In contrast, the areas of low variability associated with large bathymetric features (along the mid-ocean ridges, the Falkland and Kerguelen Plateaus, ~78°W where the PF encounters the Antarctic Peninsula, and through much of Drake Passage [see *Moore et al.*, 1997]) have strong gradients in PPV and thus relatively narrow PPV plains (compare Plates 1 and 5). Even though mean PPV changes drastically along the circumpolar path of the PF (Figure 6a), locally the PF tends to maintain a relatively constant PPV. Thus the envelope of PF paths is highly correlated with the size and shape of the local plain of quasi-constant PPV (compare Figure 1 and Plate 5).

4. Conclusions

Variability in the location and dynamics of the Antarctic Polar Front are largely a function of the underlying topography and corresponding PPV field. Over the deep ocean basins, where broad plains of quasi-constant PPV are found, the surface expression of the PF is weakened, and the PF meanders over large latitudinal ranges. Near large bathymetric features (with large gradients in PPV) the PF is intensified, and meandering is inhibited.

In regions where the PF is forced across isolines of PPV by the topography, relative vorticity is input to the water column through the shrinking/stretching of vortex lines. This relative vorticity is likely dissipated through nonlinear processes, such as eddy actions. Both width and temperature change across the PF increase in these areas. Large-scale meandering is inhibited, but mesoscale variability increases (Figures 3c and 3d).

The intensification of the PF initiated at large topographic features persists for some distance downstream. Thus elevated mesoscale variability and increased width and temperature change across the PF are seen downstream of the Pacific-Antarctic Ridge, Drake Passage, Kerguelen Plateau, and the Southeast Indian Ridge. The intensification of the PF in these areas may lead to baroclinic instabilities and increased eddy activity. It is here that we primarily observed the formation of warm and cold core rings along the PF.
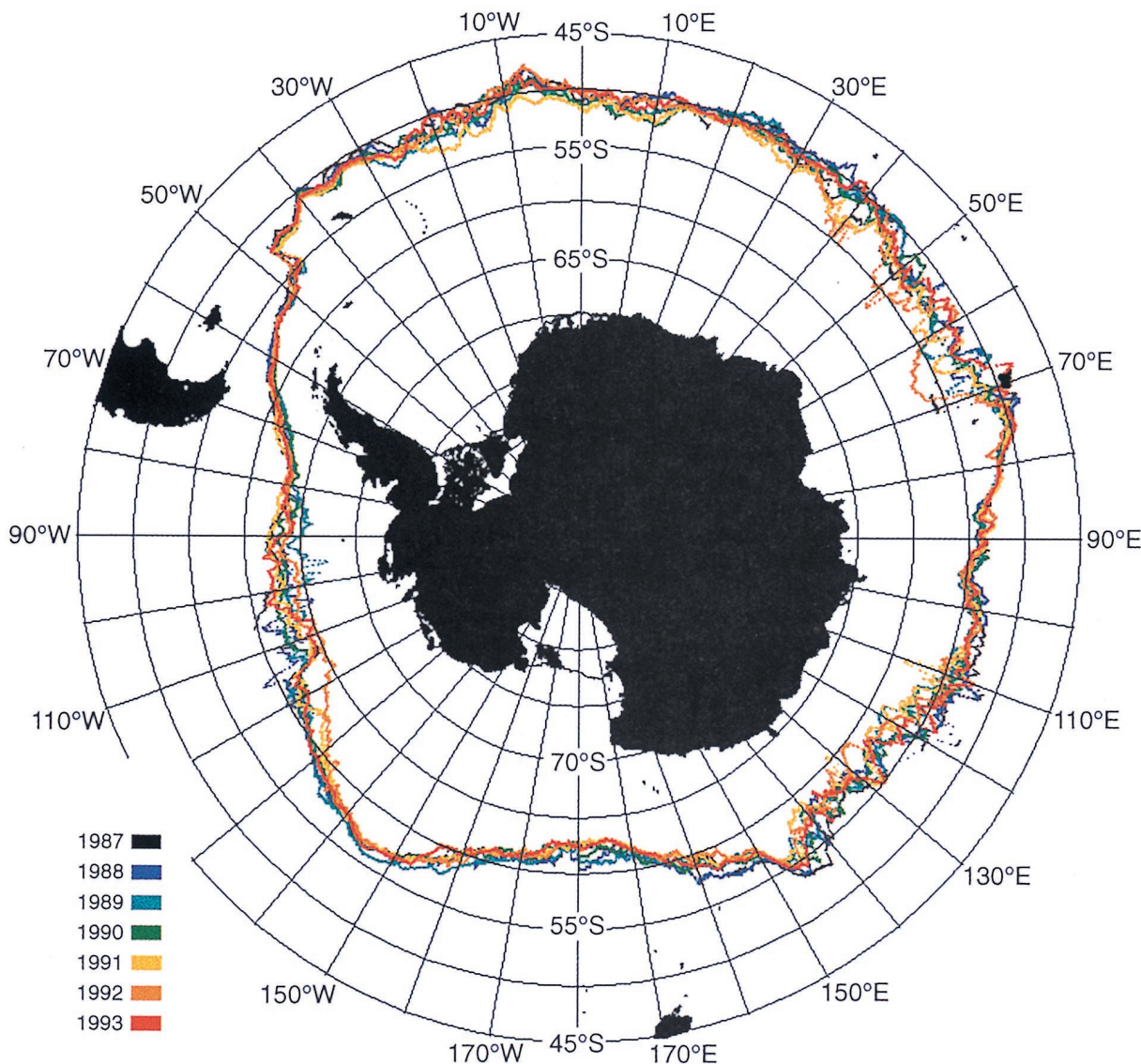
Plate 4. The mean annual path for each of the years 1987–1993 is shown.

Deacon [1937] argues that the location of the Antarctic PF is determined by the movements of Circumpolar Deep and Bottom waters. Specifically, the PF is located at the point where density isotherms associated with warm Circumpolar Deep Water bend sharply toward the surface as they move southward overriding Antarctic Bottom Water [*Deacon*, 1937]. The strong influence of topography on surface flow apparent in our results supports this hypothesis. Surface flows in the Southern Ocean can respond to mesoscale bathymetric features due to weak density stratification and relatively small Rossby Radii.

The crucial role of the topography/PPV field in constraining the dynamics of the PF implies that ocean circulation models must incorporate realistic topography at mesoscale spatial resolution before they will be able to reproduce the behavior of the PF. The close correlations between the dynamics of the PF and the underlying topography also suggest that hydrographic measurements made at several locations (including over ocean basins and in topographically controlled areas) might be extrapolated to make circumpolar calculations (i.e., of poleward heat flux, etc.).

The Antarctic PF is a circumpolar feature in the sense that it is seen at all longitudes within the Southern Ocean (Figure 1). However, the surface expression of the PF is a dynamic, regionally varying feature that is intensified near large topographic features and weakens over deep basin areas (to the point that it was frequently not detectable in our analysis, even in unobstructed, cloud-free images). *Emery* [1977] noted this weakening of ACC fronts over areas without large topographic obstructions.

The mean paths of the surface and subsurface expressions of the PF are closely coupled over much of the Southern Ocean. When surface/subsurface separations occur, the surface expression typically lies south of the subsurface expression [*Lutjeharms and Valentine*, 1984; *Sparrow et al.*, 1996; this study]. This likely reflects the fact that the thermodynamics of the two water masses makes it easier for the less dense Subantarctic waters to override denser Antarctic surface waters.

The postulated frequent surface/subsurface separations at Ewing Bank [*Moore et al.*, 1997], at the Ob'-Lena Rise [*Sparrow et al.*, 1996], and at the Udintsev Fracture Zone (this study)
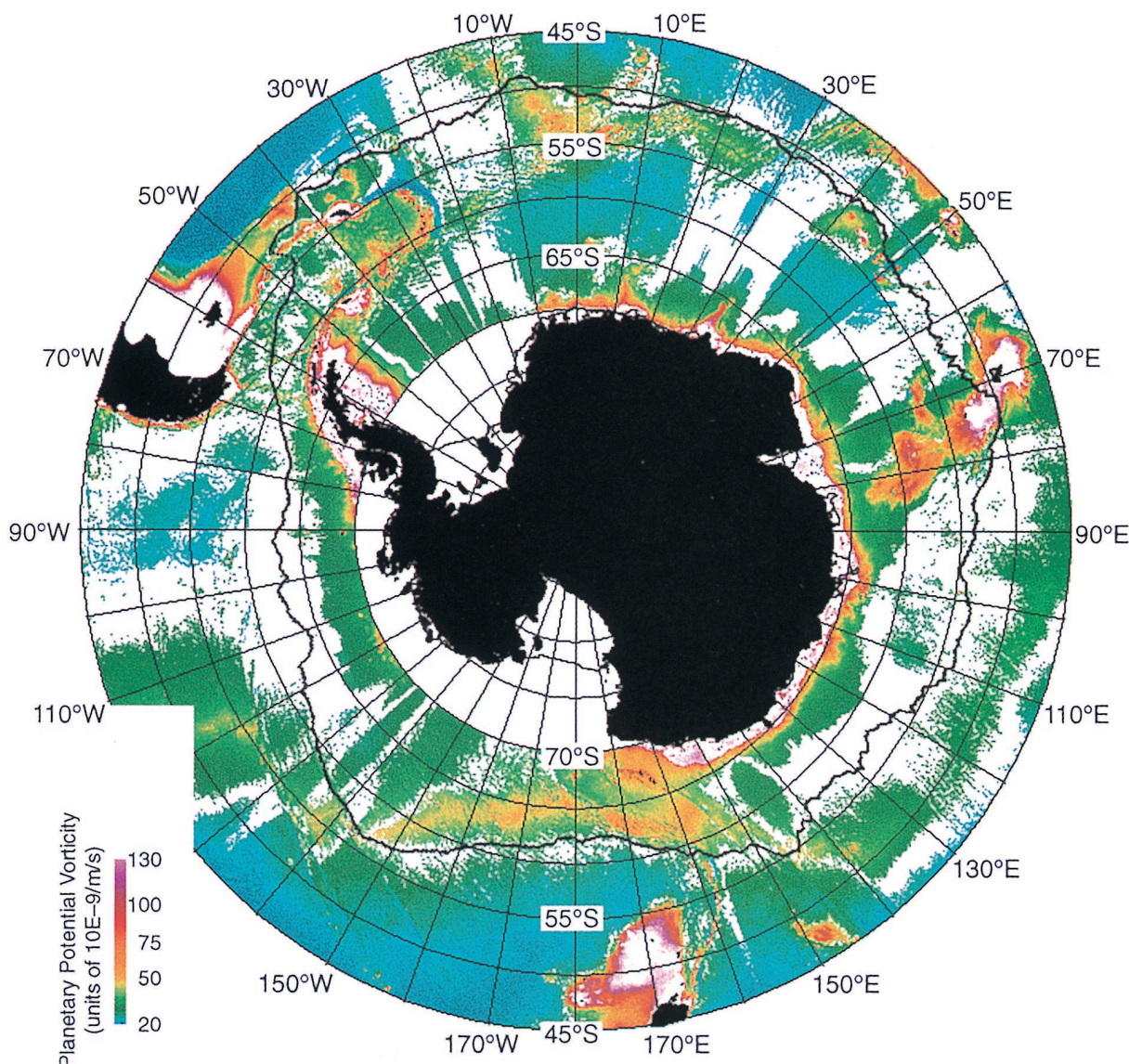
Plate 5. Mean path of the Polar Front overlain on a map of planetary potential vorticity (f/H). The mean planetary potential vorticity along the PF was calculated at each longitude from points within a moving 2° of longitude window. A range of planetary potential vorticity values consisting of the mean value 2×10^{-9} m^{-1} s^{-1} along each line of longitude is shown in white. This range corresponds to the mean value ±7%.

have some features in common. In each location the subsurface expression of the PF may be locked in place by the topography (see Plate 1). In addition, at Ewing Bank and the Udintsev Fracture Zone the SAF frequently comes into close contact with the PF, at times merging to form a single front [*Peterson and Whitworth*, 1989; this study].

Similar SAF/PF interactions occur west of the Ob'-Lena Rise near 30°E [*Orsi et al.*, 1993, 1995; *Read and Pollard*, 1993; *Belkin and Gordon*, 1996; this study]. *Gille* [1994] notes that the PF and SAF converge at ~33°E. It may be that the surface/subsurface separation described by *Sparrow et al.* [1996] is initiated west of the Ob'-Lena Rise where the PF interacts with the SAF. While our mean path (and likely the subsurface expression) lies north of the Ob'-Lena Rise, we mapped a number of PF paths over and south of the rise (Figure 1 and Plate 1).

References

Belkin, I. M., Alteration of the front distributions in the Southern Ocean near the Crozet Plateau, *Dokl. Acad. Sci. USSR, Earth Sci. Ser., Engl. Transl.*, *308*, 265–268, 1989.

Belkin, I. M., Front structure of the South Atlantic, in *Pelagicheskie Ekosistemy Yuzhnogo Okeana* (*Pelagic Ecosystems of the Southern Ocean*), (in Russian), edited by N. M. Voronina, pp. 40–53, Nauka, Moscow, 1993.

Belkin, I. M., Main hydrological features of the central South Pacific (in Russian), in *Pacific Subantarctic Ecosystems*, edited by M. E.

Vinogradov and M. V. Flint, pp. 21–28, Nauka, Moscow, 1988. (English translation, pp. 12–17, N. Z. Transl. Cent., Wellington, N. Z., 1997.)

Belkin, I. M., A. L. Gordon, Southern Ocean fronts from the Greenwich meridian to Tasmania, *J. Geophys. Res*., *101*, 3675–3696, 1996.

Botnikov, V. N., Geographic position of the Antarctic Convergence Zone in the Southern Ocean (in Russian), *Sov. Antarct. Exped. Inf. Bull*., *41*, 19–24, 1963. (*Sov. Antarct. Exped. Inf. Bull*., *Engl. Transl*., *4*, 324–327, 1963.)

Boyer, D. L., R. R. Chen, L. Tao, and P. A. Davies, Physical model of bathymetric effects on the Antarctic Circumpolar Current, *J. Geophys. Res*., *98*, 2587–2608, 1993.

Brown, J. W., O. B. Brown, and R. H. Evans, Calibration of advanced very high resolution radiometer infrared channels: A new approach to nonlinear correction, *J. Geophys. Res*., *98*, 18,257–18,268, 1993.

Burling, R. W., Hydrology of circumpolar waters south of New Zealand, *N. Z. Dep. Sci. Ind. Res. Bull*., *143*, 66, 1961.

Chelton, D. B., M. G. Schlax, D. L. Witter, and J. G. Richman, Geosat altimeter observations of the surface circulation of the Southern Ocean, *J. Geophys. Res*., *95*, 17,877–17,903, 1990.

Cornillon, P., The effect of the New England seamounts on Gulf Stream meandering as observed from satellite IR imagery, *J. Phys. Oceanogr*., *16*, 386–389, 1986.

Daniault, N., and Y. Ménard, Eddy kinetic energy distribution in the Southern Ocean from altimetry and FGGE drifting buoys, *J. Geophys. Res*., *90*, 11,877–11,889, 1985.

Deacon, G. E. R., A general account of the hydrology of the South Atlantic Ocean, *Discovery Rep*., *VII*, 177–238, 1933.

Deacon, G. E. R., The hydrology of the Southern Ocean, *Discovery Rep*., *XV*, 1–124, 1937.

Deacon, G. E. R., Kerguelen, antarctic and subantarctic, *Deep Sea Res*., *30*, 77–81, 1983.

Emery, W. J., Antarctic Polar Frontal Zone from Australia to the Drake Passage, *J. Phys. Oceanogr*., *7*, 811–822, 1977.

Gamberoni, L., J. Geronimi, P. F. Jeannin, and J. F. Murail, Study of frontal zones in the Crozet-Kerguelen region, *Oceanol. Acta*, *5*, 289–299, 1982.

Gille, S. T., Mean sea surface height of the Antarctic Circumpolar Current from Geosat data: Method and application, *J. Geophys. Res*., *99*, 18,255–18,273, 1994.

Gille, S. T., The Southern Ocean momentum balance: Evidence for topographic effects from numerical model output and altimeter data, *J. Phys. Oceanogr*., *27*, 2219–2232, 1997.

Gloersen, P., W. J. Campbell, D. J. Cavalieri, J. C. Comiso, C. L. Parkinson, and H. J. Zwally, *Arctic and Antarctic Sea Ice, 1978–1987: Satellite Passive-Microwave Observations and Analysis*, Natl. Aeronaut. and Space Admin., Washington, D. C., 1992.

Gordon, A. L., D. T. Georgi, and H. W. Taylor, Antarctic Polar Front Zone in the western Scotia Sea: Summer 1975, *J. Phys. Oceanogr*., *7*, 309–328, 1977.

Gordon, A. L., E. Molinelli, and T. Baker, Large-scale relative dynamic topography of the Southern Ocean, *J. Geophys. Res*., *83*, 3023–3032, 1978.

Gouretski, V. V., and A. I. Danilov, Weddell Gyre: Structure of the eastern boundary, *Deep Sea Res*., *Part I*, *40*, 561–582, 1993.

Gouretski, V. V., and A. I. Danilov, Characteristics of warm rings in the African sector of the Antarctic Circumpolar Current, *Deep Sea Res*., *Part I*, *41*, 1131–1157, 1994.

Guretskii, V. V., Surface thermal fronts in the Atlantic sector of the Southern Ocean, *Sov. Meteorol. Hydrol*., *Engl. Transl*., *8*, 67–73, 1987.

Hansen, D. V., and G. A. Maul, A note on the use of sea surface temperature for observing ocean currents, *Remote Sens. Environ*., *1*, 161–164, 1970.

Hofmann, E. E., The large-scale horizontal structure of the Antarctic Circumpolar Current from FGGE drifters, *J. Geophys. Res*., *90*, 7087–7097, 1985.

Houtman, T. J., Surface temperature gradients at the Antarctic Convergence, *N. Z. J. Geol. Geophys*., *7*, 245–270, 1964.

Hughes, C. W., Rossby waves in the Southern Ocean: A comparison of TOPEX/POSEIDON altimetry with model predictions, *J. Geophys. Res*., *100*, 15,933–15,950, 1995.

Hughes, C. W., The Antarctic Circumpolar Current as a waveguide for Rossby waves, *J. Phys. Oceanogr*., *26*, 1375–1387, 1996.

Hughes, C. W., and P. D. Killworth, Effects of bottom topography in the large-scale circulation of the Southern Ocean, *J. Phys. Oceanogr*., *25*, 2485–2497, 1995.

Ikeda, Y., G. Siedler, and M. Zwierz, On the variability of Southern Ocean front locations between Southern Brazil and the Antarctic Peninsula, *J. Geophys. Res*., *94*, 4757–4762, 1989.

Inoue, M., Modal decomposition of the low-frequency currents and baroclinic instability at Drake Passage, *J. Phys. Oceanogr*., *15*, 1157–1181, 1985.

Johnson, J. A., and R. B. Hill, A three-dimensional model of the Southern Ocean with bottom topography, *Deep Sea Res*., *22*, 745–751, 1975.

Joyce, T. M., W. Zenk, and J. M. Toole, The anatomy of the Antarctic Polar Front in the Drake Passage, *J. Geophys. Res*., *83*, 6093–6113, 1978.

Killworth, P. D., An equivalent-barotropic mode in the Fine Resolution Antarctic Model, *J. Phys. Oceanogr*., *22*, 1379–1387, 1992.

Klyausov, A. V., Position of the South Polar Front near Kerguelen and Heard Islands in the autumn of 1987, *Oceanology, Engl Transl*., *30*, 142–148, 1990.

Koblinsky, C. J., The global distribution of f/H and the barotropic response of the ocean, *J. Geophys. Res*., *95*, 3213–3218, 1990.

Laubscher, R. K., R. Perisinotto, and C. D. Mcquaid, Phytoplankton production and biomass at frontal zones in the Atlantic sector of the Southern Ocean, *Polar Biol*., *13*, 471–481, 1993.

Lee, T., and P. Cornillon, Temporal variation of meandering intensity and domain-wide lateral oscillations of the Gulf Stream, *J. Geophys. Res*., *100*, 13,603–13,613, 1995.

Legeckis, R., Oceanic Polar Front in the Drake Passage: Satellite observations during 1976, *Deep Sea Res*., *24*, 701–704, 1977.

Lutjeharms, J. R. E., Location of frontal systems between Africa and Antarctica: Some preliminary results, *Deep Sea Res*., *Part A*, *32*, 1499–1509, 1985.

Lutjeharms, J. R. E., and D. J. Baker Jr., A statistical analysis of the meso-scale dynamics of the Southern Ocean, *Deep Sea Res*., *Part A*, *27*, 145–159, 1980.

Lutjeharms, J. R. E., and A. Foldvik, The thermal structure of the upper ocean layers between Africa and Antarctic during the period December 1978 to March 1979, *S. Afr. J. Antarct. Res*., *16*, 13–20, 1986.

Lutjeharms, J. R. E., and L. H. McQuaid, Changes in the structure of thermal ocean fronts south of Africa over a three-month period, *S. Afr. J. Sci*., *82*, 470–476, 1986.

Lutjeharms, J. R. E., and H. R. Valentine, Southern Ocean thermal fronts south of Africa, *Deep Sea Res*., *Part A*, *31*, 1461–1475, 1984.

Mackintosh, N. A., The Antarctic Convergence and the distribution of surface temperatures in Antarctic waters, *Discovery Rep*., *XXIII*, 177–212, 1946.

Moore, J. K., M. R. Abbott, and J. G. Richman, Variability in the location of the Antarctic Polar Front (90°–20°W) from satellite sea surface temperature data, *J. Geophys. Res*., *102*, 27,825–27,833, 1997.

Morrow, R., R. Coleman, J. Bhurch, and D. Chelton, Surface eddy momentum flux and velocity variances in the Southern Ocean from Geosat altimetry, *J. Phys. Oceanogr*., *24*, 2050–2071, 1994.

Nowlin, W. D., Jr., and J. M. Klinck, The physics of the Antarctic Circumpolar Current, *Rev. Geophys*., *24*, 469–491, 1986.

Olson, D. B., O. B. Brown, and S. R. Emmerson, Gulf Stream frontal statistics from Florida Straits to Cape Hatteras derived from satellite and historical data, *J. Geophys. Res*., *88*, 4569–4577, 1983.

Orsi, A. H., W. D. Nowlin Jr., T. Whitworth III, On the circulation and stratification of the Weddell Gyre, *Deep Sea Res*., *Part I*, *40*, 169–203, 1993.

Orsi, A. H., T. Whitworth III, and W. D. Nowlin Jr., On the meridional extent and fronts of the Antarctic Circumpolar Current, *Deep Sea Res*., *Part I*, *42*, 641–673, 1995.

Park, Y. H., L. Gamberoni, and E. Charrlaud, Frontal structure, water masses, and circulation in the Crozet Basin, *J. Geophys. Res*., *98*, 12,361–12,385, 1993.

Patterson, S. L., Surface circulation and kinetic energy distribution in the Southern Hemisphere oceans from FGGE drifting buoys, *J. Phys. Oceanogr*., *15*, 865–884, 1985.

Patterson, S. L., and T. Whitworth, Physical Oceanography, in *Antarctic Sector of the Pacific*, edited by G. P. Glasby, pp. 55–93, Elsevier, New York, 1990.

Peterson, R. G., and T. Whitworth III, The Subantarctic and Polar Front in relation to deep water masses through the southwestern Atlantic, *J. Geophys. Res*., *94*, 10,817–10,838, 1989.

Pratt, L. J., Critical control of zonal jets by bottom topography, *J. Mar. Res*., *47*, 111–130, 1989.

Read, J. F., and R. T. Pollard, Structure and transport of the Antarctic Circumpolar Current and Agulhas Return Current at 40°E, *J. Geophys. Res.*, *98*, 12,281–12,295, 1993.

Read, J. F., R. T. Pollard, A. I. Morrison, and C. Symon, On the southerly extent of the Antarctic Circumpolar Current in the southeast Pacific, *Deep Sea Res.*, *Part II*, *42*, 933–954, 1995.

Robertson, J. E., and A. J. Watson, A summer-time sink for atmospheric carbon dioxide in the Southern Ocean between 88°W and 80°E, *Deep Sea Res.*, *Part II*, *42*, 1081–1091, 1995.

Sandwell, D. T., and B. Zhang, Global mesoscale variability from the Geosat exact repeat mission: Correlation with ocean depth, *J. Geophys. Res.*, *94*, 17,971–17,984, 1989.

Schlich, R., M. F. Coffin, M. Munschy, H. M. J. Stagg, Z. G. Li, and K. Revill, *Bathymetric Chart of the Kerguelen Plateau*, Inst. de Phys. du Globe, Strasbourg, France, 1987.

Sciremammano, F. Jr., R. D. Pillsbury, W. D. Nowlin Jr., and T. Whitworth III, Spatial scales of temperature and flow in Drake Passage, *J. Geophys. Res.*, *85*, 4015–4028, 1980.

Sievers, H. A., and W. D. Nowlin Jr., The stratification and water masses at Drake Passage, *J. Geophys. Res.*, *89*, 10,489–10,514, 1984.

Smith, E., J. Vasquez, A. Tran, and R. Sumagaysay, Satellite-derived sea surface temperature data available from the NOAA/NASS Pathfinder Program, *Eos Trans. AGU Electron. Suppl.*, 1996. (Available as http://www.agu.org/eos_elec/95274e.html)

Smith, W. H. F., and D. T. Sandwell, Bathymetric prediction from dense satellite altimetry and sparse shipboard bathymetry, *J. Geophys. Res.*, *99*, 21,803–21,824, 1994.

Sparrow, M. D., K. J. Heywood, J. Brown, and D. P. Stevens, Current structure of the south Indian ocean, *J. Geophys. Res.*, *101*, 6377–6391, 1996.

Tsuchiya, M., L. D. Talley, and M. S. McCartney, Water-mass distributions in the western South Atlantic: A section from South Georgia Island (54S) northward across the equator, *J. Mar. Res.*, *52*, 55–81, 1994.

Witter, D. L., and D. B. Chelton, Eddy-mean flow interactions induced by modulations of zonal ridge topography in a Quasi-Geostrophic Channel Model, *J. Phys. Oceanogr.*, *28*, 2019–2039, 1998.

M. R. Abbott, J. K. Moore, and J. G. Richman, College of Oceanic and Atmospheric Sciences, Oregon State University, 104 Ocean Administrative Building, Corvallis, OR 97331-5503. (mabbott@oce.orst.edu; jmoore@oce.orst.edu;richman@oce.orst.edu)